

# Complex folding pathways in a simple $\beta$ -hairpin

Guanghong Wei,<sup>1</sup> Normand Mousseau,<sup>1,\*</sup> and Philippe Derreumaux<sup>2,3</sup>

<sup>1</sup>*Département de physique et GCM, Université de Montréal,  
C.P. 6128, succ. centre-ville, Montréal (Québec) Canada*

<sup>2</sup>*Information Genomique et Structurale, CNRS-UMR 1889,  
31 Chemin Joseph Aiguier, 13402 Marseille Cedex 20, France*

<sup>3</sup>*Laboratoire de Biochimie Theorique, UPR 9080 CNRS,*

*Institut de Biologie Physico-Chimique, 13 rue Pierre et Marie Curie, 75005 Paris, France*

(Dated: October 30, 2018)

The determination of the folding mechanisms of proteins is critical to understand the topological change that can propagate Alzheimer and Creutzfeld-Jakobs diseases, among others. The computational community has paid considerable attention to this problem; however, the associated time scale, typically on the order of milliseconds or more, represents a formidable challenge. *Ab initio* protein folding from long molecular dynamics (MD) simulations or ensemble dynamics is not feasible with ordinary computing facilities and new techniques must be introduced. Here we present a detailed study of the folding of a 16-residue  $\beta$ -hairpin, described by a generic energy model and using the activation-relaxation technique. From a total of 90 trajectories at 300 K, three folding pathways emerge. All involve a simultaneous optimization of the complete hydrophobic and hydrogen bonding interactions. The first two follow closely those observed by previous theoretical studies. The third pathway, never observed by previous all-atom folding, unfolding and equilibrium simulations, can be described as a reptation move of one strand of the  $\beta$ -sheet with respect to the other. This reptation move indicates that non-native interactions can play a dominant role in the folding of secondary structures. These results point to a more complex folding picture than expected for a simple  $\beta$ -hairpin.

**Key words:** the Activation-Relaxation Technique; protein folding; simulations;  $\beta$ -hairpin; reptation.

PACS numbers:

## INTRODUCTION

As one of the smallest building blocks of proteins, the  $\beta$ -hairpin and particularly the second  $\beta$ -hairpin of the domain B1 of protein G (referred to as  $\beta$ -hairpin2) has been the subject of many theoretical and experimental folding studies. This peptide adopts hairpin structures in solution but overall its flexibility precludes the determination of a high-resolution NMR solution structure. [1] Fluorescence experiments show that this  $\beta$ -hairpin folds in isolation with a time constant of 6 microseconds and its folding kinetics is described by the two-state model. [2] Because these data do not provide details of the transition and such a time scale cannot be covered by hundreds of long molecular dynamics (MD)-trajectories at 300 K in explicit solvent, [3] alternative methods have been used in order to characterize the thermodynamics and folding kinetics of the  $\beta$ -hairpin2.

Two folding mechanisms have already been proposed. The first mechanism, suggested by statistical mechanical models [4] and lattice Monte Carlo (MC) simulations, [5] is that folding starts at the turn and propagates towards the tail by hydrogen bonding interactions, the hydrophobic cluster forming at the end of folding. One variant of this mechanism suggested by Langevin

dynamics of an off-lattice model is that the formation of the hydrophobic cluster is followed by zipping of hydrogen bonds (H-bonds), predominantly starting from those near the turn. [6] Another variant suggested by all-atom MD simulations is that the  $\beta$ -hairpin folds beginning at the turn, followed by hydrophobic collapse and then H-bond formation. [7]

The second mechanism proposed is that the N- and C-termini first approach each other to form a loop, and the structure propagates from there. This mechanism is apparently independent of all-atom force field details, since it has been recognized by ensemble dynamics at 300 K using implicit solvent, [8] replica exchange method combining MD trajectories with a temperature exchange MC process using SPC model solvent, [9] minimalist Go-folding discontinuous MD simulations, [10] unfolding simulations, [11, 12] and multicanonical MC simulations with an implicit solvent model. [13]

Along with the difference in folding dynamics within each scenario, three questions are yet to be resolved. The first question is when the native H-bond network and hydrophobic core form: (i) the hydrophobic core is being formed first, and the H-bonds appear, [11, 12, 13, 14, 15] (ii) the H-bonds form first and then the hydrophobic core, [2] or (iii) the final hydrophobic core and H-bonds form simultaneously. [6, 8, 10] The second question is whether helical structures exist during folding process. Berne et al., by using the OPLSAA force field, did not find evidence of significant helical structures in their

---

\*Electronic address: Normand.Mousseau@umontreal.ca

simulations at all temperatures studied, [9] while Garcia and Sanbonmatsu found a helical content of 15% at low temperatures, [14] Pande et al. detected short-lived semi-helical intermediates at room temperature, [8] and Irbäck found a low population of  $\alpha$ -helix structure at 273 K. [16] The third question is whether the previously used methods, which fail to detect both pathways, may miss other major folding pathways, as has been discussed recently [17] for ensemble dynamics which uses a large number of short MD simulations of only tens of nanoseconds and a supercluster of thousands of computer processors.

To address these issues, we simulate the folding mechanisms of hairpin2 using a previously described model — the Optimized Potential for Efficient peptide-structure Prediction (OPEP), and sampling technique — the Activation-Relaxation Technique (ART). [18, 19] OPEP can be used to simulate any amino acid sequence and works for proteins that do and do not form ordered structures in solution. Ordered structures include three-helix bundles and three-stranded anti-parallel  $\beta$ -sheet structures, among others. [20] For its part, ART generates trajectories on the configurational energy landscape, identifying a series of energy minima separated by first-order saddle points. The efficiency of ART is not affected by the height of the activation energy barriers or the complexity of the atomic rearrangements and thus samples very efficiently the rugged-energy landscapes of small proteins. The OPEP-ART approach has been applied recently to study the folding of three sequences adopting an  $\alpha$ -helix, a three stranded antiparallel  $\beta$ -sheet and a  $\beta$ -hairpin helix in solution. [21] In this work, 82 folding simulations at 300 K start from a fully extended conformation ( $\phi = -180^\circ$ ,  $\psi = 180^\circ$ ) using different random-number seeds: 52 use the standard OPEP force field (16 reaching the folded state), 20 use a modified set of OPEP parameters (6 reaching the folded state), and 10 use a biased Go-like potential (10 reaching the folded state). To determine the effect of the starting structure, we also launched 8 independent runs (4 reaching the folded state) at 300 K starting from a semi-helical conformation using the standard OPEP force field.

From a total of 90 trajectories at room temperature, 36 found the native state providing a detailed picture of the folding mechanism. Although all these folding trajectories involve a simultaneous optimization of the complete hydrophobic and hydrogen bonding interactions, the 36 folding runs can be described by 3 mechanisms: two of them follow closely those observed by previous theoretical and computational studies, but the third one represents a new folding mechanism for proteins. This mechanism can be described as a reptation move of one strand of the  $\beta$ -sheet with respect to the other. These three mechanisms offer a complete picture of the  $\beta$ -hairpin folding, independently of the exact amino acid composition, and help reconcile conflicting theoretical data on the hairpin2 of protein G [2, 6, 10, 13] or between various hairpins, e.g., the first hairpin of tendamistat [22] and a 11-residue model peptide. [23] The existence of these three compet-

ing mechanisms was presented recently in a short communication; [24] here, we offer a detailed description of the folding mechanisms in this simple  $\beta$  hairpin. Furthermore, we present the results of new simulations using either G $\bar{o}$ -like potential or semi-helical starting conformations.

## METHODS

We have simulated the folding of the C-terminal  $\beta$ -hairpin from protein G (residues 41-56). The sequence of the peptide is GEWTYDDATKTFVTE. The energy surface was modeled using the OPEP model and the dynamics was obtained by the activation-relaxation technique.

### Activation-Relaxation Technique

ART is a generic method to explore the landscape of continuous energy functions through a series of activated steps. The algorithm has evolved considerably over the years and here we apply its most recent version, ART nouveau, [25, 26] which uses a recursion method, the Lanczós algorithm, [27] to extract the direction of lowest curvature of the landscape leading to a first-order saddle point. Such an approach provides an efficient way to extract a limited spectrum of eigenvectors and eigenvalues without requiring the evaluation and diagonalization of the full Hessian matrix. A similar approach was also introduced in Ref. 28. An ART event is defined directly in the space of configurations, which allows for moves of any complexity, and consists of four steps:

1. Starting from a local minimum, a configuration is first pushed outside the harmonic well until a negative eigenvalue appears in the Hessian matrix.
2. The configuration is then pushed along the eigenvector associated with the negative eigenvalue until the total force is close to zero, indicating a saddle point. The first two steps constitute the activation phase.
3. The configuration is pushed slightly over the saddle point and is relaxed to a new local minimum, using standard minimization technique.
4. Finally, the new configuration is accepted/rejected using the Metropolis criterion at the desired temperature. In each of the simulations at hand, this four-step procedure was repeated 4000 times, taking less than 18 processor-hours on an IBM Power-4 machine

As discussed in our previous work, [21] the temperature in ART is not a real temperature since ART samples the conformational space from one minimum to another

minimum. However, ART generates well-controlled trajectories (more than 83% of events relax back to within 0.4 Å from their initial minima starting at the saddle points). [21] A detailed description of the algorithm and implementation of ART can be found in earlier publications. [18, 19, 21]

### Energy Model

We use a coarse-grained off-lattice model where each amino acid is represented by its N, H, C $\alpha$ , C, O and one bead for its side chain. The exact OPEP energy function, which includes solvent effects implicitly, was obtained by maximizing the energy of the native fold and an ensemble of non-native states for six training peptides with 10-38 residues. In this work, the side chain propensities of the 20 amino acids for  $\alpha_R$  helix,  $\beta$ -strand and  $\alpha_L$  helix [29, 30] are neglected. The total energy is thus expressed by:

$$E = w_L E_L + w_H E_{HB1} + w_{HH} E_{HB2} + w_{SC,SC} E_{SC,SC} + w_{SC,M} E_{SC,M} + w_{M,M} E_{M,M} \quad (1)$$

The interaction potential OPEP is a function of the weights  $w$ 's of the following interactions:

- (i) quadratic terms to maintain stereochemistry: bond lengths and bond angles for all particles and improper dihedral angles for the side chains and the peptide bonds  $E_L$ ,
- (ii) and excluded-volume potential of the main chain interactions  $E_{M,M}$  and of side chain-main chain interactions  $E_{SC,M}$ ,
- (iii) pairwise contact 6-12 interactions between the side chains considering all 20 amino acid types  $E_{SC,SC}$ ,
- (iv) backbone two-body  $E_{HB1}$  and four-body  $E_{HB2}$  hydrogen bonding interactions. All nonbonded interactions are included (no truncation).

The two-body energy of one H-bond between residues  $i$  and  $j$  is defined by

$$E_{HB1} = \varepsilon_{hb} \sum_{ij} \mu(r_{ij}) \nu(\alpha_{ij}) \quad (2)$$

where

$$\mu(r_{ij}) = 5 \left( \frac{\sigma}{r_{ij}} \right)^{12} - 6 \left( \frac{\sigma}{r_{ij}} \right)^{10} \quad (3)$$

$$\nu(\alpha_{ij}) = \begin{cases} \cos^2 \alpha_{ij} & \alpha_{ij} > 90^\circ \\ 0 & \text{otherwise} \end{cases} \quad (4)$$

where  $r_{ij}$  is the O..H distance between the carbonyl oxygen and amide hydrogen and  $\alpha_{ij}$  the NHO angle.

The cooperative energy between two neighbored H-bonds  $ij$  and  $kl$  is defined by

$$E_{HB2} = \varepsilon_{2hb} \exp(-(r_{ij} - \sigma)^2/2) \exp(-(r_{kl} - \sigma)^2/2) \Delta(ijkl) \quad (5)$$

where  $\Delta(ijkl) = 1$  if  $(k,l) = (i+1, j+1)$  or  $(i+2, j-2)$  or  $(i+2, j+2)$ , otherwise  $\Delta(ijkl) = 0$ . This corresponds to the pattern of H-bonds in  $\alpha$ -helices, anti-parallel and parallel beta-sheets, respectively.

In this work, unless specified we use  $\sigma = 1.8$  Å,  $\varepsilon_{hb} = 1.0$  kcal/mol if  $j=i+4$  (helix), otherwise = 1.5 kcal/mol, and  $\varepsilon_{2hb} = -2.0$ . The other parameters can be found in Ref. 20.

### Trajectory Analysis

Our native structure contains six main chain H-bonds excluding the one at the turn since it rarely forms because of geometrical constraints. Following Karplus [13] and Garcia, [14] they are numbered from the tail to the turn 42:HN-55:O (H1), 55:HN-42:O (H2), 44:HN-53:O (H3), 53:HN-44:O (H4), 46:HN-51:O (H5), 51:HN-46:O (H6). The expression  $i$ :HN- $j$ :O denotes the atoms involving a H-bond between residues  $i$  and  $j$ .

To characterize a conformation, we use the number of native H-bonds, the radius of gyration of the hydrophobic core ( $R_{g_{core}}$ ), and the  $C_\alpha$ -rmsd of residues 41-56 from the 2GB1 structure.[31]  $R_{g_{core}}$  is calculated using the side chains of the four residues W43, Y45, F52, and V54. A H-bond is defined if it satisfies DSSP conditions: [32] the distance between the carbonyl oxygen and amide hydrogen (O..H) is less than 2.4 Å and the NHO angle is greater than 145°.

The regions of conformational space that have been sampled by all simulations are clustered as follows. The  $C_\alpha$ -rmsd is calculated for each pair of structures in each simulation. The number of neighbors is then computed for each structure using a  $C_\alpha$ -rmsd cutoff of 1.5 Å. The conformation with the highest number of neighbors is considered as the center of the first cluster. All the neighbors of this conformation are removed from the ensemble of conformations. The center of second cluster is then determined in the same way as for the first cluster, and this procedure is repeated until each structure is assigned to a cluster. Then we have a list of central structures of clusters for every folding simulation. Once all the trajectories are clustered, we can cluster all the central structures in two different folding trajectories, in order to identify the common clusters between the simulations.

## RESULTS

### Native vs. Non-native Hairpin Structures

Cluster analysis of all ART-generated trajectories shows that the lowest-energy conformation ( $E = -33$  kcal/mol) deviates by less than 1 Å  $C_\alpha$  rms from the hairpin structure within protein G (PDB code 2GB1 [31]). For the purpose of our simulation, we define a structure as being fully folded – or native – if it

satisfies the following four criteria: (i) the six native H-bonds are formed (see Methods); (ii) the backbone dihedral angles ( $\phi$ ,  $\psi$ ) have standard  $\beta$ -sheet values (around  $(-90^\circ, 150^\circ)$ ); (iii) the hydrophobic core is well packed (core radius of gyration is around 4.3 Å) and (iv) the all-residue  $C_\alpha$  rmsd from 2GB1 is less than 2.5 Å. These conditions for nativeness are thus more stringent than those of in previous folding simulations. [8, 10] For Zagrovic and collaborators, [8] the H-bonds connecting the two strands are not required to be native and hairpin with asymmetric strands are considered as native structures. Similarly, for Zhou *et al*, [10] the condition for nativeness is that all-heavy atom rmsd from the global minimum structure is less than 2.5 Å. The rmsd between their modeled structure and the experimental 2GB1 is not given.

Figure 1 (produced by using the MOLMOL software [33]) shows the 2GB1 structure (a), our native structure (b) and six non-native hairpin structures (c-h) sampled by ART. Figure 1(e) and 1(h) show two hairpins in which the turn (residues 7-11) is shifted toward C terminus. Figure 1(f) and 1(g) show two non-native hairpins where the turn (residues 6-10) is shifted toward the N terminus. In this study, only hairpin (b), of lowest energy, is the native state, while, according to the definition of folded state in Ref. 8, hairpin structures (c)-(h) are also folded states. Our hairpin structures (c) and (d) are very similar to the folded state in Series 17 (two key H-bonds are HB53-44 and HB52-45) and Series 2 (two key H-bonds are HB45-52 and HB43-54) of Ref. 8, respectively. Both of them have symmetric strands, but different H-bond network pattern. Moreover, from the key H-bonds in their eight independent folding trajectories, it seems that the hairpin structures in Series 1, 7, 9, 11 are asymmetric about the  $\beta$ -turn.

### Analysis of Unfolded Trajectories

From a total of 90 runs, 36 trajectories reach the native state. The other 54 fail to locate the native structure within 4000 ART-events. These runs lead either to non-native hairpin conformations as discussed previously or to other metastable conformations of various secondary compositions, e.g.  $\alpha$ -helix with coil, three-stranded antiparallel  $\beta$ -sheet and short  $\alpha$ -helix with  $\beta$ -like structures.

Figure 2 shows the structural features of the 8 lowest energy metastable structures sampled. The 54 metastable states lie between  $-21$  and  $-30$  vs.  $-33$  kcal/mol for the native state. It is important to note that these structures do not represent dead ends for the simulation; continuing the simulation at 300 K for two arbitrarily chosen metastable states (c) and (d), we find that it is possible to reach the fully formed hairpin structure within 5000 additional trial events. In Fig. 3, we plot the energy vs. rmsd for the lowest-energy structures in all the 52 simulations (16 folded and 36 unfolded) using the standard OPEP and starting from the fully extended state.

We see that all folded structures appear in a dense region around  $-33$  kcal/mol and below an rmsd of 2.0 Å and are well separated from the non-folded ones; clearly, our potential can discriminate folded states from metastable states. By visual inspection of the 36 metastable states and comparison with Fig. 3, we see (i) that the conformations with  $E$  between  $-25$  and  $-30$  kcal/mol and rmsd between 2.0 and 4.1 Å adopt asymmetric  $\beta$ -sheet structures with different H-bond networks, (ii) that the conformations with  $E$  between  $-25$  and  $-28$  kcal/mol and rmsd between 6.0 and 8.5 Å show three-stranded antiparallel  $\beta$ -sheet structures, (iii) and that the other conformations with  $E$  between  $-21$  and  $-25$  kcal/mol and rmsd between 3.0 and 8.0 Å adopt  $\alpha$ -helix with coil, short  $\beta$ -hairpin with coil, or short  $\alpha$ -helix with  $\beta$ -like structures. As the rmsd of some non-native hairpin structures can be as small as 2.1 Å (see Fig. 2(b)), it is clear that this sole criterion is not sufficient to differentiate between native and non-native hairpin structures.

### Analysis of Folded Trajectories

As reported in Ref. 24, the 16 folding simulations using the standard OPEP potential which start from a fully extended state can be classified into 3 mechanisms : I (4 runs), II (7 runs) and III (5 runs).

A detailed analysis of mechanism I, seen in four folding trajectories, is given in Figure 4. This mechanism is similar to that described in Refs. 5, 6, 23. Starting from a fully extended state, the peptide first collapses into a compact state with the turn placed in the right section of the chain (residues 7-10) (Events 53); this step is characterized by the formation of a partially packed hydrophobic core (radius of gyration of the hydrophobic core,  $Rg_{core}$ , is 4.8 Å, see Fig. 4(b)) and the appearance of several non-native H-bonds (Fig. 4(c)). The following steps serve to stabilize its hydrophobic core. At event 80, a native H-bond near the turn (H5) forms, followed rapidly by the formation of H4; 29 events later (event 109), the peptide reorganizes its hydrophobic core to a well packed state ( $Rg_{core}$  reaches its final value 4.3 Å). The reorganization of the hydrophobic core allows the formation of new native main chain H-bonds (H3, H2, H6). At that point, the two-end distance fluctuates around 9 Å (Fig. 4(b)). In spite of these new native H-bonds, the flexibility of the loop remains large and H6, an H-bond near the loop, breaks and reforms many times between events 128 and 300 (see Run 1 in Fig. 5). Finally, the H-bond H1, near the end of the peptide, forms at last (event 471) leading to the native state: the core radius of gyration remains its final value 4.3 Å, the rmsd from 2GB1 structure drops to 2.0 Å (Fig. 4(b)), the total number of native H-bonds is six, and the total energy is  $-32$  kcal/mol (Fig. 4(c)). The time formation of the six native H-bonds H1-H6 can be seen in Fig. 5 for the four folding runs. The number of native and non-native H-bonds in each accepted conformation as a function of

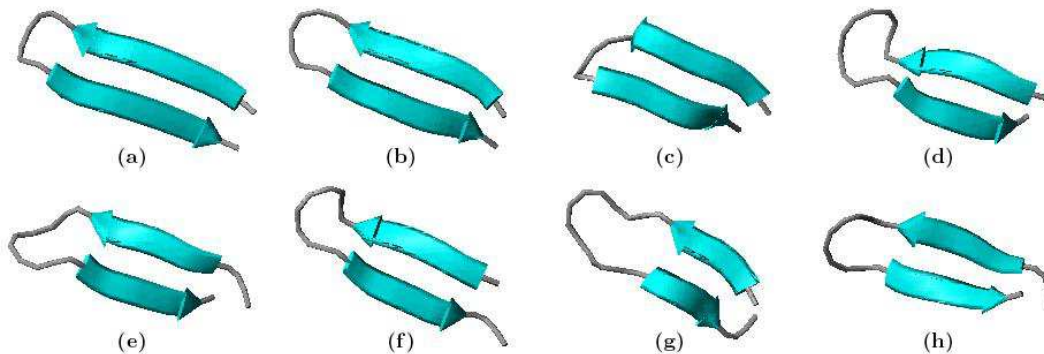


FIG. 1: The sampled hairpin structures with different main chain H-bonds and 2GB1 structure. (a) 2GB1 structure; (b) Hairpin structure with 6 native H-bonds (H1-H6), rmsd = 1.09 (0.88) Å, E = -33 kcal/mol; (c) hairpin structure with 5 key H-bonds (H1-H4, 52:HN-45:O), rmsd = 2.87 (2.15) Å, E = -29 kcal/mol; (d) hairpin structure with 4 key hydrogen bonds (43:HN-54:O, 45:HN-52:O, 52:HN-45:O, 54:HN-43:O), rmsd = 2.62 (2.39) Å, E = -28 kcal/mol; (e) hairpin structure with 4 key H-bonds (44:HN-54:O, 46:HN-52:O, 52:HN-46:O, 54:HN-44:O), rmsd = 2.08 (1.87) Å, E = -30 kcal/mol; (f) hairpin structure with 5 key H-bonds (43:HN-53:O, 45:HN-51:O, 51:HN-45:O, 53:HN-43:O, 45:HN-41:O), rmsd = 2.42 (2.18) Å, E = -29 kcal/mol; (g) hairpin structure with 4 key H-bonds (42:HN-54:O, 44:HN-52:O, 52:HN-44:O, 54:HN-42:O), rmsd = 2.40 (1.98) Å, E = -28 kcal/mol; (h) hairpin structure with 4 key H-bonds (43:HN-55:O, 45:HN-53:O, 53:HN-45:O, 55:HN-43:O), rmsd = 3.56 (2.96) Å, E = -28 kcal/mol. The rmsd value in parentheses is the  $C_{\alpha}$ -rmsd from 2GB1 for residues 43-54. According to our definition of folded state, only hairpin (b) is folded state.

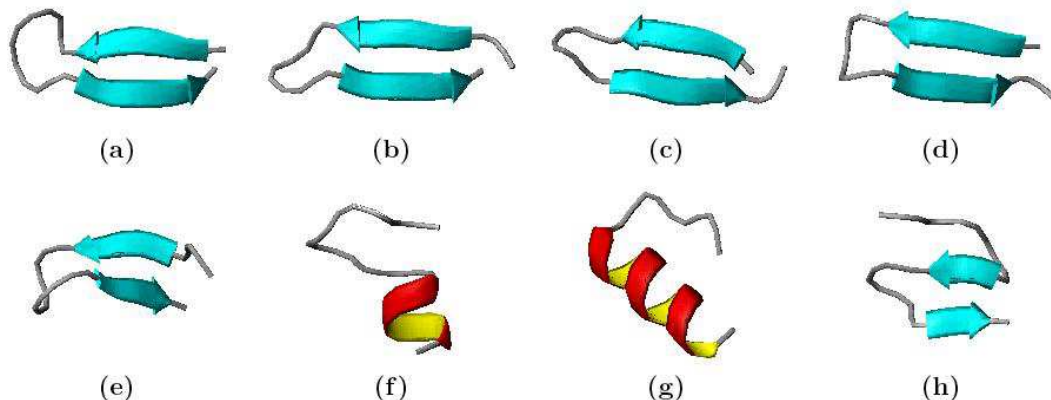


FIG. 2: The sampled metastable states using the standard OPEP potential, starting from a fully extended state. (a) hairpin structure with 4 key H-bonds (43:HN-54:O, 45:HN-52:O, 52:HN-45:O, 54:HN-43:O), rmsd = 2.62 Å, E = -28 kcal/mol; (b) hairpin structure with 4 key H-bonds (44:HN-54:O, 46:HN-52:O, 52:HN-46:O, 54:HN-44:O), rmsd = 2.08 Å, E = -30 kcal/mol; (c) hairpin structure with 4 key H-bonds (44:HN-54:O, 46:HN-52:O, 52:HN-46:O, 54:HN-44:O), rmsd = 2.88 Å, E = -27 kcal/mol; (d) hairpin structure with 5 key H-bonds (43:HN-53:O, 45:HN-51:O, 51:HN-45:O, 53:HN-43:O, 45:HN-41:O), rmsd = 2.6 Å, E = -29 kcal/mol; (e) hairpin structure with 4 key H-bonds (44:HN-55:O, 46:HN-53:O, 53:HN-46:O, 55:HN-44:O), rmsd = 3.34 Å, E = -23 kcal/mol; (f) a  $\alpha$ - $\beta$  structure with short helix appearing in the C terminal, rmsd = 7.39 Å, E = -22 kcal/mol; (g) an  $\alpha$ -helix structure involving residues from 5 to 15, rmsd = 5.89 Å, E = -23 kcal/mol; (h) a three-stranded beta-sheet structure with 4 H-bonds (42:HN-49:O, 49:HN-42:O, 48:HN-54:O, 54:HN-48:O), rmsd = 7.81 Å, E = -27 kcal/mol. Two metastable state (c) and (d) converge to the native state within 5000 additional trial events.

event number is given in Fig. 4(c). We clearly see that the folding process is a competition between native and non-native hydrogen bonding interactions, and that in Mechanism I the two ends of this  $\beta$ -hairpin gradually come near to form H1 last, and the hydrophobic core becomes well packed rapidly.

Mechanism II, seen in seven folding trajectories, was observed in simulations of hairpin2 [8, 9, 13] and of a 10-residue model peptide. [34] Figure 6 shows the major

folding steps associated with this mechanism. Within a few events, the hydrophobic interaction between the four residues W43, Y45, F52, and V54 induces the formation of a partial hydrophobic core ( $Rg_{core}$  is 6.4 Å) resulting in a globular state with three non-native H-bonds (event 55). At the same time, the N- and the C-termini approach each other to form a large loop. Because of the competition between the hydrophobic, native, and non-native hydrogen bonding forces, the peptide rear-

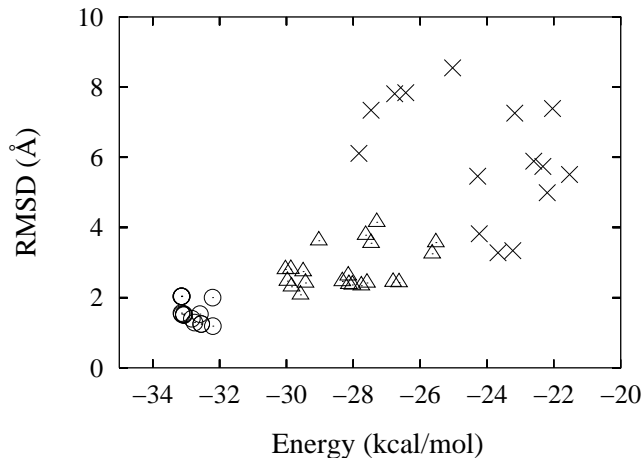


FIG. 3: Rmsd as a function of energy of the lowest-energy structures generated in the 52 simulations (16 folded and 36 unfolded) using the standard OPEP potential, starting from a fully extended state. Circles, triangles, and crosses are for native  $\beta$ -hairpin, asymmetric  $\beta$ -hairpin with different H-bond pattern, and other different structures, respectively.

ranges its hydrophobic core by breaking and reforming some non-native interactions ( $Rg_{core}$  increases to 8 Å). At event 191, the hydrophobic core drops to 5.5 Å and, after 16 more events, the H-bond H1 (event 207) near the end forms. This reorganization of hydrophobic core causes the second (H2 at event 366) and third (H3 at event 417) H-bonds to form. After a 150-event optimization between hydrophobic and hydrogen bonding interactions, the radius of gyration of the hydrophobic core reaches its final value (4.3 Å at event 567), and the fourth H-bond H4 appears. In the following several events, H5 (at event 570) and H6 (at event 573) form; the peptide satisfies the native conditions (see Fig. 6). Fig. 7 shows the time formation of the six native H-bonds H1-H6 in the seven folding trajectories. As is shown in Fig. 6 and Fig. 7 the two ends of this  $\beta$ -hairpin come near to form H-bond H1 first (and to a lesser extent H2 first), and the hydrophobic core reorganizes to its well packed state slowly. The partial helical structure (Events 169 and 280) is not a necessary intermediate and appears in 4 of the 7 trajectories following mechanism II. Comparing the two mechanisms, one can see that they are not mutually incompatible; many trajectories fall somewhere in between these two descriptions. In some cases, for example, folding is initiated in the middle region (H4). The  $\beta$ -sheet then propagates first outwards (forming H1-H3) and then inwards (forming H5-H6) (see Run 6 in Fig. 7).

Mechanism III had not been observed in previous all-atom folding, [8, 10] unfolding, [11] and equilibrium simulations. [9, 13, 14] This mechanism, seen in five folding trajectories, is characterized by a rapid folding into a collapsed state with a turn at the wrong place, form-

ing an asymmetric hairpin structure stabilized by non-native H-bonds and a partially packed hydrophobic core. Then slowly, step by step in a reptation mode, the asymmetry is corrected, with non-native H-bonds breaking and reforming, in a structure getting closer to the native hairpin. A representative trajectory is given in Fig. 8. Folding begins with the formation of a compact state defined by a partially packed hydrophobic core and two non-native H-bonds 46:HN-55:O and 48:HN-53:O (event 55). Then the number of non-native H-bonds increases to four: 46:HN-55:O, 48:HN-53:O, 53:HN-48:O, 55:HN-46:O, and a short  $\beta$ -sheet structure (Event 84) appears. Driven by the hydrophobic interactions, at event 99, the reptation motion of the loop causes the four non-native H-bonds to break, and four new non-native H-bonds 44:HN-55:O, 46:HN-53:O, 53:HN-46:O, 55:HN-44:O form. This peptide shows a new asymmetric  $\beta$ -sheet structure, which is closer to its symmetric  $\beta$ -hairpin structure. During the next 200 events, this peptide stays in this state and reorganizes its hydrophobic core. After an optimization of the hydrophobic and hydrogen bonding interactions, at event 302, the reptation motion of the loop enhances longitudinal motion of the two strands, breaking the four non-native H-bonds and forming four native ones (H1-H4); simultaneously, the core radius of gyration drops to 4.7 Å. The hairpin structures forms rapidly afterwards, with the addition of the fifth and sixth native H-bond (H5 and H6), a rmsd dropping to 1.4 Å (Event 334), and the energy approaching to -33 kcal/mol. Once the native hairpin forms, it is fairly stable: the total number of H-bonds remains at six, the radius of gyration of the hydrophobic core keeps around 4.3 Å, the rmsd fluctuates around 1.4 Å, and the energy fluctuates around -33 kcal/mol. As shown in Figure 8 and Fig. 9, the critical and rate-limiting step in this mechanism is the breaking, almost in synchrony, of four or five non-native H-bonds of a structure very close to the native state, followed by a rapid formation of the native H-bonds. It can also be seen from Fig. 8 that the two ends of this  $\beta$ -hairpin slowly come near, and the hydrophobic core reorganizes to its well packed state slowly.

## DISCUSSION

### Sensitivity of Trajectories

Because various interaction potentials have led previously to conflicting reports regarding the details of folding, it is essential to determine how changes in the force-field and the starting structure affect the folding trajectories.

We consider here two variations of the force field. Firstly, we run 20 simulations using OPEP with an energy parameter for the H-bond  $\epsilon_{hb}$  increased from the standard value of 1.5 to 2.5, a change which could considerably affect the stability of intermediate structures. Re-

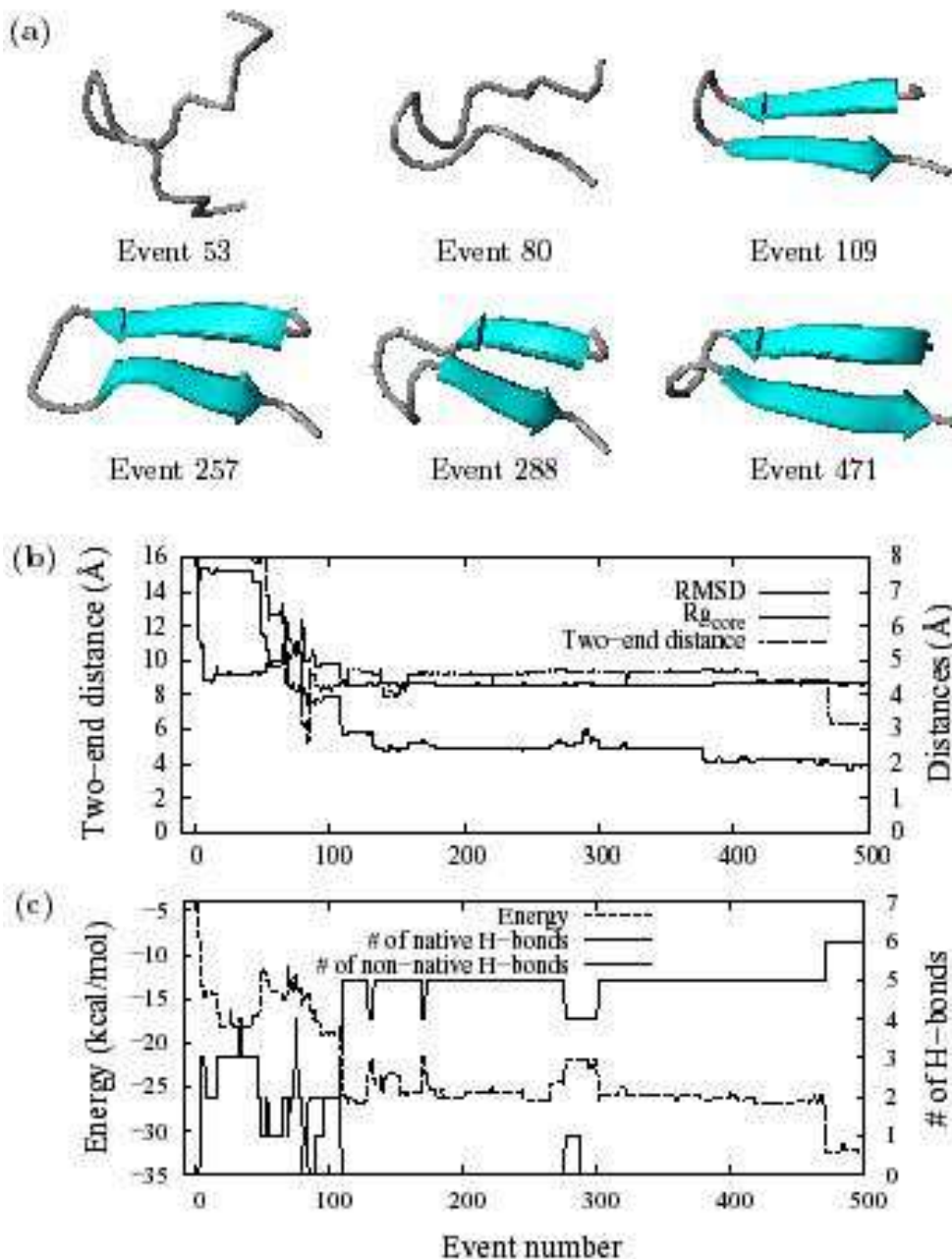


FIG. 4: Detailed analysis of a representative folding trajectory following Mechanism I, simulated at 300 K, starting from a fully extended state. (a) Six snapshots. Only accepted events are shown. (b)  $C_{\alpha}$ -rmsd from 2GB1 structure of the hairpin, radius of gyration of the hydrophobic core  $Rg_{core}$ , and the two-end distance as a function of accepted event number. (c) Total energy, number of all the native and non-native H-bonds in each sampled conformation as a function of accepted event number.

markably, we still recover the three folding mechanisms among the six successful trajectories. Secondly, we run 10 simulations using ART with G $\bar{o}$ -like OPEP potential ( $E = E(\text{OPEP}) + k * (\text{rmsd}^2)$ , for  $k = 0.5, 0.55$  and  $0.6$ ) which favors native contacts in the total energy. Starting from a fully extended state, all ten simulations found the folded state following either mechanism I or II: six simulations fold from the end region (H1 or H2 form first), two from the middle (H3 forms first) and two from the turn (H5 first). As in earlier G $\bar{o}$ -model simulations, [10]

we find no helical intermediates in any of the ten folding simulations. In these simulations, folding can be initiated at the end region, middle region, and turn region of the peptide, in agreement with the results obtained by using only the OPEP potential. Because native interactions are strongly favored in G $\bar{o}$ -model simulations, the asymmetric conformations found in mechanism III become prohibitive, preventing the appearance of mechanism III. The bias of the G $\bar{o}$  potential can therefore lead to an incomplete sampling of the folding paths.



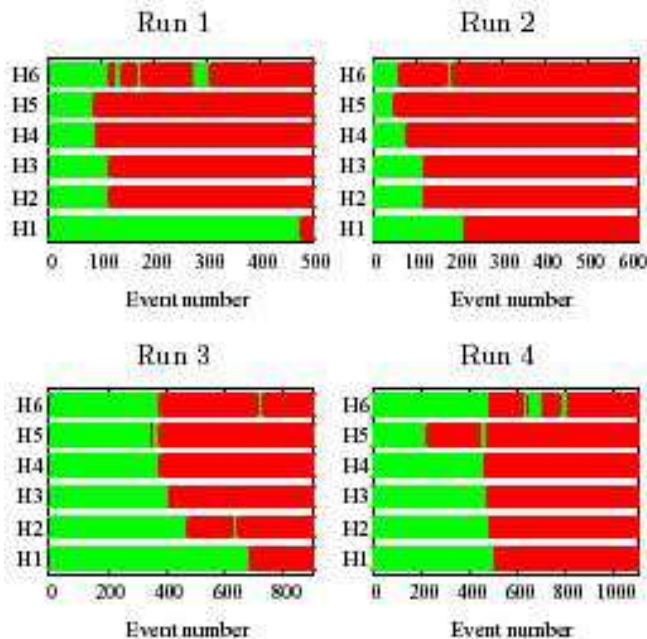


FIG. 5: Status of the six native H-bonds as a function of accepted event number in the four runs following Mechanism I. Green: not formed, red: formed. Run 1 is the simulation described in Fig. 4.

To determine the impact of the starting conformation on the ART-trajectories and to address the question of semi-helical intermediates during folding, [8] eight trial simulations were attempted at 300 K starting from a semi-helical structure. Four of those resulted in hairpin structures with six native H-bonds, while the remaining four displayed helical structures or  $\beta$ -hairpin structures with non-native H-bonds. Interestingly, the four folded trajectories closely follow Mechanism II. Figure 10 gives a representation of folding simulation at 300 K. The semi-helical structure rapidly relaxes to a more compact structure (event 92) in which the two ends of the peptide approach each other. At this stage, a partially packed hydrophobic core ( $Rg_{core}$  is 6.7 Å) appears, without native H-bonds, however. Driven by the strong hydrophobic interactions among the four hydrophobic residues (Tyr45, Phe52, Trp43, Val54), the two ends of the peptide come nearer and one native H-bond (H1) is formed at the end region of the peptide. After 50 events, the next two H-bonds H2 and H3 form almost simultaneously. The peptide stays in this state for 350 events, reorganizing slowly the hydrophobic core ( $Rg_{core}$  oscillates around 5.2 Å and the rmsd from the 2GB1 structure reaches a plateau (4 Å)). After a slow structural adjustment process, the hydrophobic core forms fully in a large cooperative move at event 500 ( $Rg_{core}$  drops to 4.3 Å), and the six native H-bonds set in rapidly afterwards (H4 and H5 form first, followed by the formation of H6). This event marks the completion of the folding process of the peptide with the rmsd reaching to 1.5 Å. This demonstrates that ART

can find the folded state starting from a helical structure and that this helical structure may exist in the real folding pathway of this protein, as discussed in previous simulations [8, 14, 16] and recent energy landscape characterization of  $\beta$ -hairpin2 and its isomers [35].

From the structure of the initial helical state, we can explain why the four folded trajectories only follow Mechanism II. This state is characterized by a helical structure spanning residues 47-50, and two non-native H-bonds (50:HN-46:O and 51:HN-47:O). The existence of this helical segment makes it difficult to form native H-bonds at the turn or the middle region of the peptide because of geometric restrictions. However the two ends of this peptide are very flexible, driven by the hydrophobic interactions, they can approach each other easily, then form a H-bond first between them. When the initial state is a fully extended state, this peptide has much more freedom to find its native state, and this is why multiple folding pathways are present.

#### Cluster Analysis of the Folded Trajectories

As we have seen in the previous section, the folding process can be described by a single concept: the competition between three types of interactions. A cluster analysis shows, however, that this does not mean that the folding trajectories can be unified.

We perform a cluster analysis following the procedure described in Ref. 36 (see Methods), using a  $C_{\alpha}$ -rmsd cutoff of 1.5 Å. All the accepted conformations in each folded trajectory of the 26 folding simulations obtained by the standard OPEP potential are used for this procedure. A total of 12-40 clusters were found for each folded trajectory, indicating strong variations in the details of the folding trajectories. Moreover, we find very little overlap of the basins between similar trajectories: except for the trivial initial and native clusters, it is generally not possible to match more than one or two clusters between trajectories following the same mechanisms. We obtained the same qualitative results using other clustering analysis.

The failure of cluster analysis by  $C_{\alpha}$ -rmsd to characterize the three different folding mechanisms for this  $\beta$ -hairpin is due to the flexibility of this small peptide. For example, the asymmetric  $\beta$ -hairpin structures in the folding trajectory following the reptation mechanism are very diverse, presenting a wide range of hydrogen-bond patterns. Moreover, the  $C_{\alpha}$ -rmsd between a beta hairpin with the turn shifted to C-terminal and a beta hairpin with the turn shifted to N-terminal is as big as 4.3 Å. Increasing the  $C_{\alpha}$ -rmsd cutoff will make it difficult to differentiate asymmetric  $\beta$ -hairpin state from the folded state. The classification in terms of folding mechanisms as identified by the formation of hydrogen bonds appears therefore superior to the clusterization method for this small peptide.



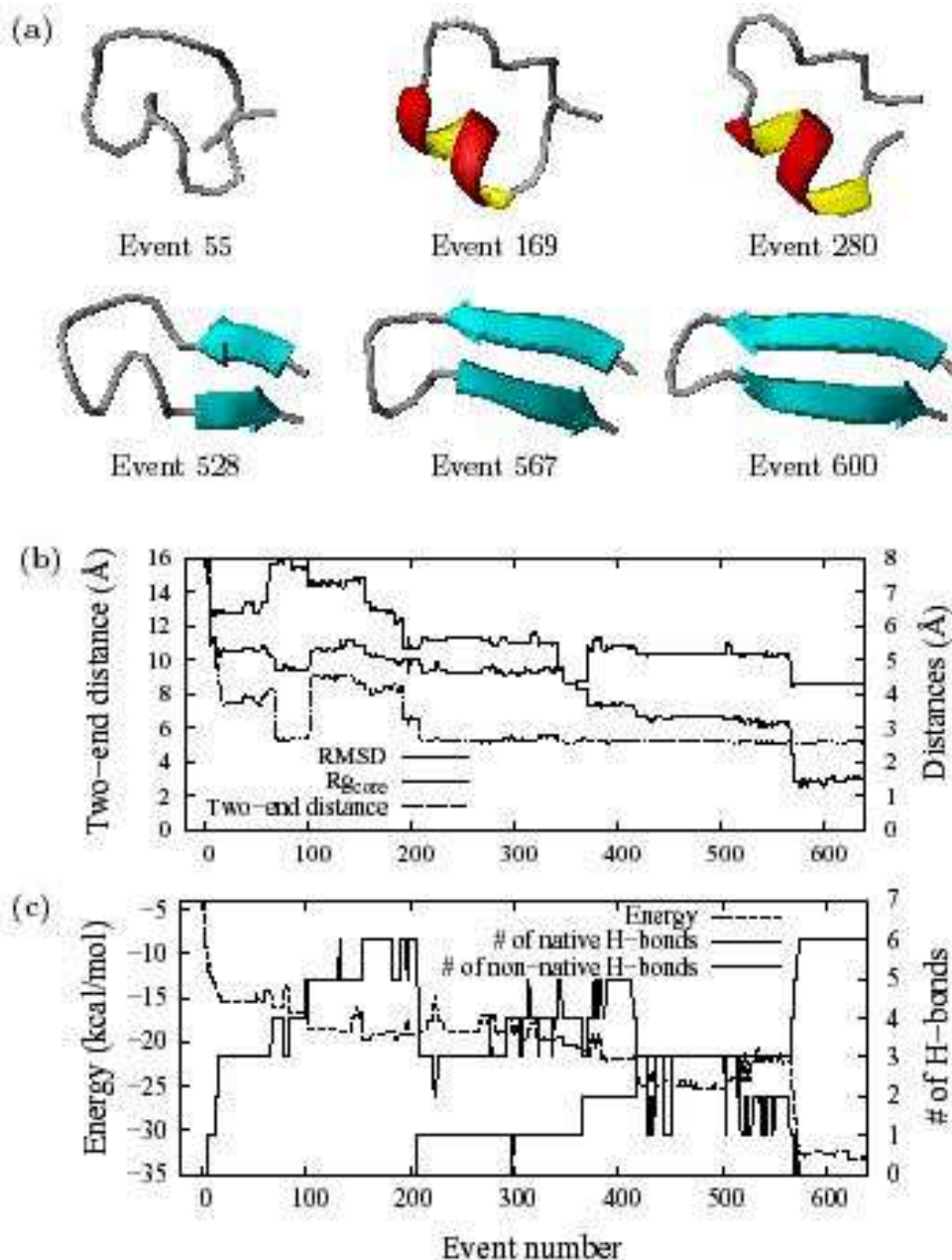


FIG. 6: Detailed analysis of a representative folding trajectory following Mechanism II, simulated at 300 K, starting from a fully extended state. (a) Six snapshots. (b)  $C_{\alpha}$ -rmsd from 2GB1 structure of the hairpin, radius of gyration of the hydrophobic core  $Rg_{core}$ , and the two-end distance as a function of accepted event number. (c) Total energy, number of all the native and non-native H-bonds in each sampled conformation as a function of accepted event number.

### Does the Reptation Folding Trajectory Exist?

Surprisingly, although present in part in many previous simulations, the reptation mechanism had not been identified previously. The asymmetric conformations with only non-native H-bonds, which characterize the intermediate states in Mechanisms III, are found in many simulations. For example, a cluster analysis of the structures produced in an all-atom multicanonical MC simulation of the  $\beta$ -hairpin2 finds that these asymmetric conformations account for 20% of all conformations. [13]

Similarly, Skolnick and collaborators find that a lattice model often folds into asymmetric structures. [5] In a recent work of Irbäck, a local minimum corresponding to a  $\beta$ -hairpin with non-native topology is observed in the energy landscape of this  $\beta$ -hairpin2. [16] Finally, most of the folded conformations identified by Zagrovic *et al.* in distributed MD simulations (Folding@home) seem asymmetric although this is not explicitly stated. [8] Similar results are found in smaller peptides such as the 11-residue model peptide of Wang *et al.* studied by molecular dynamics, which also displays asymmetric  $\beta$ -hairpin

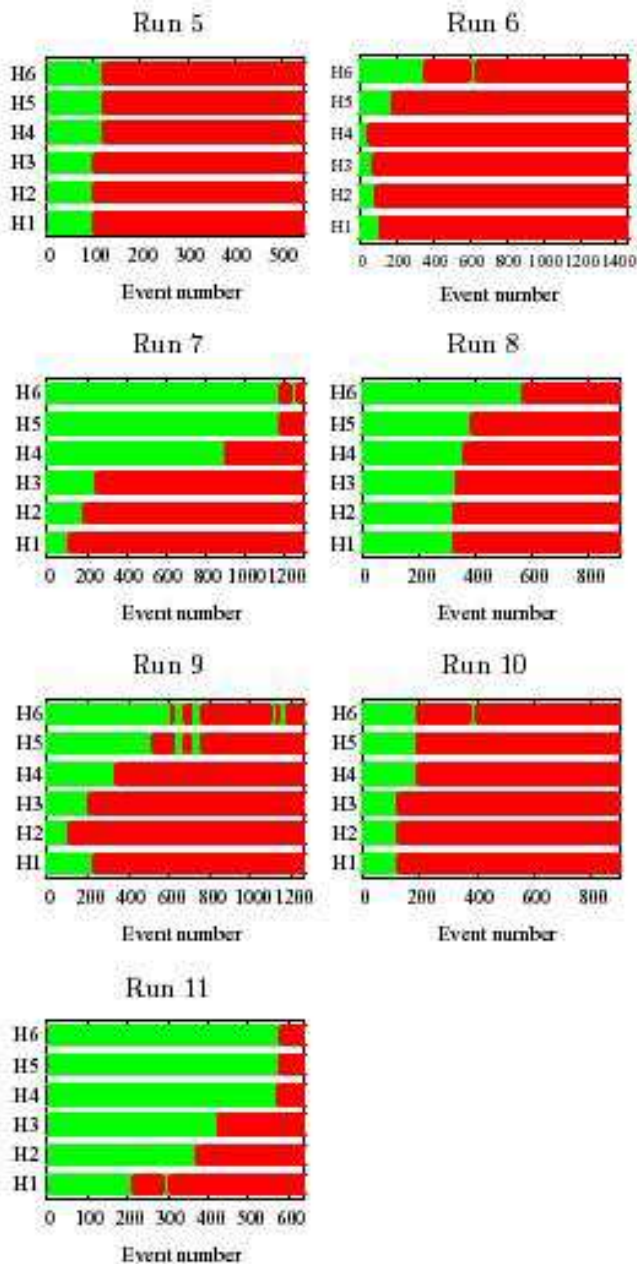


FIG. 7: Status of the six native H-bonds as a function of accepted event number in the seven runs following Mechanism II. Green: not formed, red: formed. Run 11 is the simulation described in Fig. 6.

structures. [23]

Although many simulations found the asymmetric conformation, none seems to have been able to overcome the rate-limiting step, which requires breaking all non-native bonds at once (Fig. 9 (b)), in order to form the native state. With OPEP, this barrier is found to be about 12 kcal/mol and corresponds to a time scale on the order of  $\mu\text{s}$ , [37] near the experimental folding time but much beyond what can be reached by standard molecular dy-

namics.

In addition to display a time scale in agreement with experiment, there is experimental evidence that many  $\beta$ -hairpin sequences can populate two distinct hairpin conformations of various loop lengths and pairings of  $\beta$ -strands in solution. [38, 39] Fluorescence microscopy also suggests that myosin can induce the reptation of actin filaments when adenosine triphosphate is added. [40] The reptation mechanism, which has been well established as a fundamental movement in polymer chain, might therefore exist in the folding of a simple  $\beta$ -hairpin.

### Competition between Hydrophobic and Native Hydrogen Bonding Interactions

The folding mechanisms described above are the result of a strong competition between hydrophobic and native hydrogen-bonding interactions. All cases show that the hydrophobic interactions play a dominant role in the folding process. At the beginning of the folding, a partially packed hydrophobic core always forms before native H-bonds appear (see Fig. 4(b) and (c), Fig. 6(b) and (c), Fig. 8(b) and (c), Fig. 10(b) and (c)). The following step is the rearrangement of the hydrophobic core and the optimization between the complete hydrophobic and native hydrogen bonding interactions. When hydrophobic and hydrogen bonding interactions reach a balance, the well packed hydrophobic core forms before (Fig. 4(b) and (c)) or at the same time as (Fig. 6(b) and (c), Fig. 8(b) and (c), Fig. 10(b) and (c)) the native H-bonds network forms.

### Competition between Native and Non-native Hydrogen Bonding Interactions

Native and non-native hydrogen-bonding interactions also compete strongly during the folding process. The initial collapse is always accompanied by the formation of three to six non-native H-bonds (see Fig. 4(c), Fig. 6(c), Fig. 9(b), Fig. 10(c)). However, these non-native H-bonds are not stable in the long run; they form, break, and reform in response to the movement of the hydrophobic core. Driven by the hydrophobic interactions, the non-native hydrogen bonding interactions finally become weaker, and native H-bonds form, leading rapidly to the native state. The whole folding process can therefore be described as a balance between hydrophobic, native and non-native hydrogen bonding forces.

## CONCLUSIONS

By demonstrating that the folding of a  $\beta$ -hairpin can be initiated at the end, the middle and the turn region, as well as from an asymmetric conformation, the three folding mechanisms proposed here help reconcile conflicting

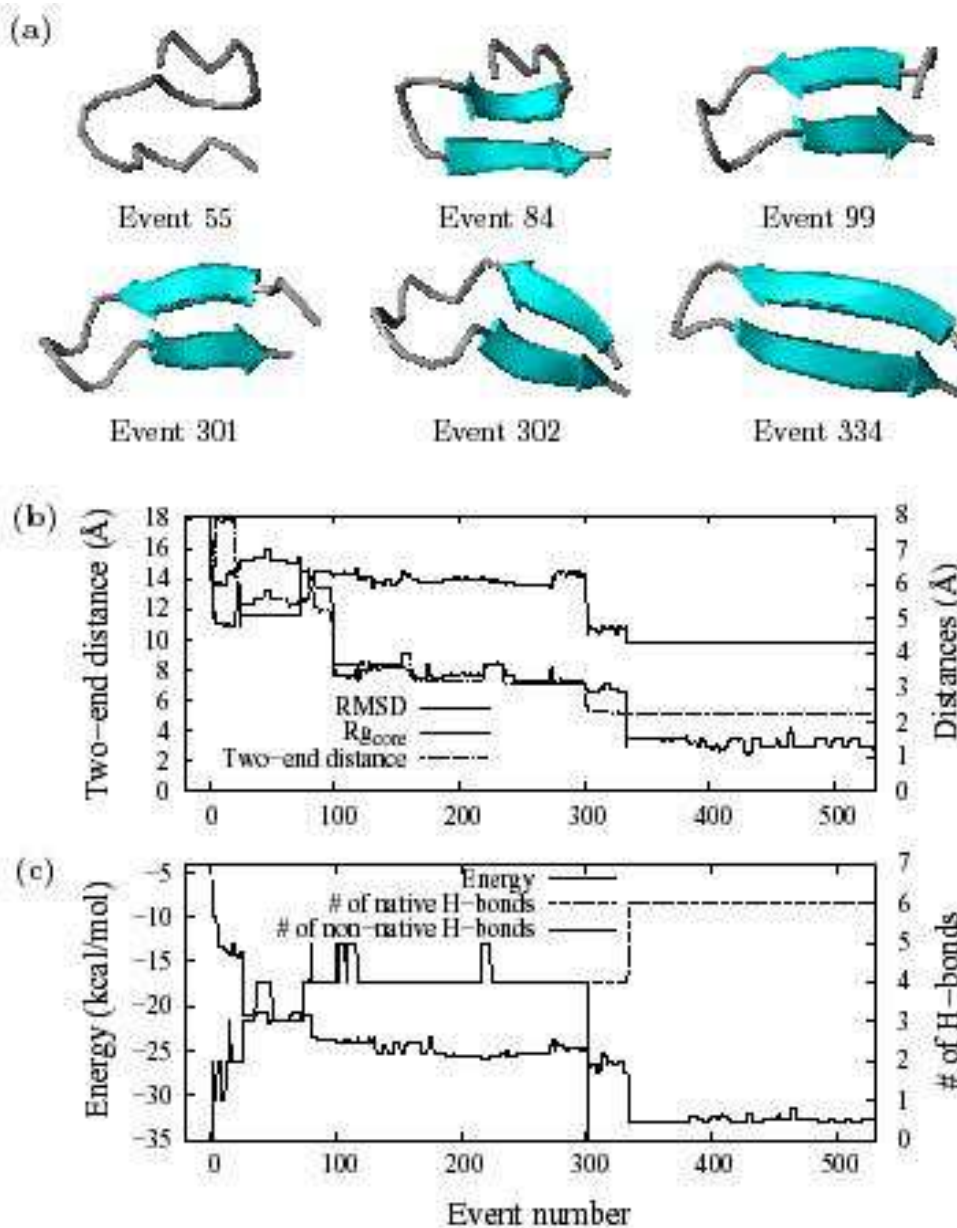


FIG. 8: Detailed analysis of a folding trajectory following Mechanism III, simulated at 300 K, starting from a fully extended state. Another folding trajectory was presented in a short communication. [24] (a) Six snapshots. (b)  $C_{\alpha}$ -rmsd from 2GB1 structure of the hairpin, radius of gyration of the hydrophobic core  $Rg_{core}$ , and the two-end distance as a function of accepted event number. (c) Total energy, number of all the native and non-native H-bonds in each sampled conformation as a function of accepted event number.

theoretical data on the hairpin2 of protein G [2, 6, 10, 13] or between various hairpins, e.g. the first hairpin of tendamistat. [22] Using these three mechanisms, we can now propose a complete picture of the folding of  $\beta$ -hairpins which does not depend on the exact amino-acid composition. The exact folding path followed by a given  $\beta$ -hairpin should be influenced by its sequence and the solvent conditions; all paths should, however, belong to one of the three mechanisms presented here. The first two mechanisms, with the propagation from either the turn or the end points, had already been described in

previous reports on  $\beta$ -hairpin 2, but no previous method had managed to detect both pathways. The third mechanism, identified in these simulations for the first time, involves folding into an asymmetric state followed by a reptation of one strand over the other until the peptide reaches its native state. The existence of this mechanism is supported by a number of experimental and numerical results even though the rate-limiting step and the presence of non-native states place it outside the scope of most simulation methods, including unfolding, G $\ddot{o}$  and standard MD approaches. This last results underlines the

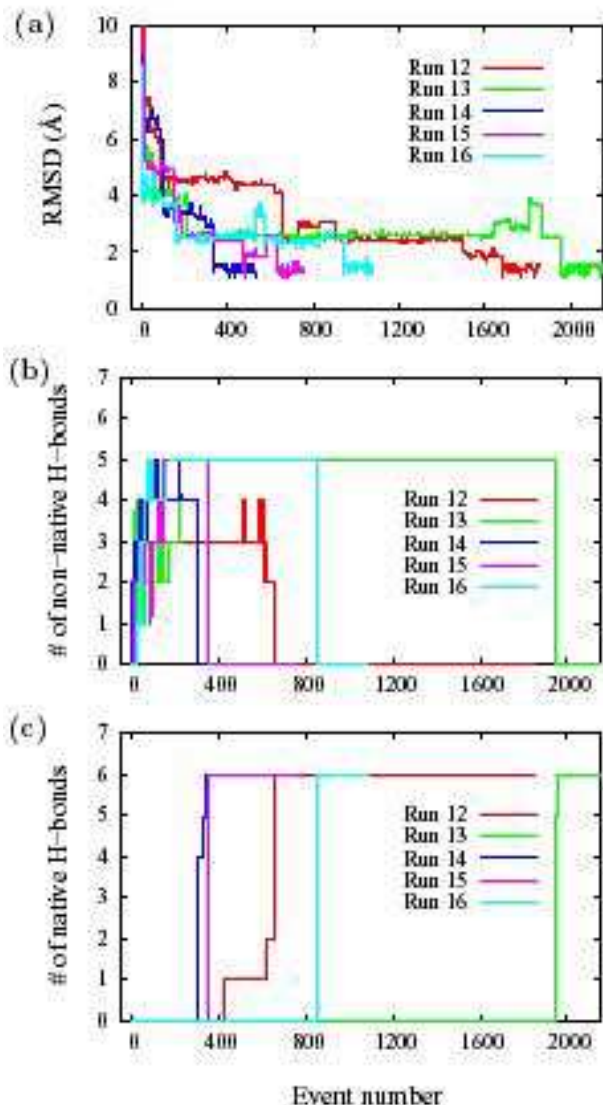


FIG. 9: Analysis of all trajectories following Mechanism III. (a) Rmsd from the 2GB1 structure, (b) number of non-native H-bonds, and (c) number of native H-bonds in each conformation as a function of accepted event number. Run 13 is the the folding simulation described in Fig. 3 in a short communication, [24] and Run 14 is the folding simulation described in Fig. 8. The final rmsd's from the 2GB1 structure are less than 1.8 Å (see (a)) in the five folding simulations. In the five folding simulations, on average, the non-native H-bonds break almost at the same time (see(b)), then the native H-bonds form rapidly, almost instantaneously (see(c)).

importance of direct non-biases methods, such as ART, for studying the folding process.

Although complex, presenting a large number of different paths, the folding of this  $\beta$ -hairpin can still be described by a unique process of competition between hydrophobic core and native and non-native H-bond interactions. In particular, it is clear that non-native H-bond interactions can play a critical role in the folding process even though they are absent in the final product.

## ACKNOWLEDGEMENTS

GW and NM are supported in part by the *Fonds québécois pour la formation des chercheurs et l'aide à la recherche* and the *Natural Sciences and Engineering Research Council* of Canada. Most of the calculations were done on the computers of the *Réseau québécois de calcul de haute performance (RQCHP)*. NM is a Cottrell Scholar of the Research Corporation. We thank Drs. Hue Sun Chan, Marek Cieplak, and Saraswathi Vishveshwara for useful discussion.

[1] Blanco FJ, and Serrano L. Folding of protein GB1 domain studied by the conformational characterization of fragments comprising its secondary structure elements. *Eur J Biochem* 1999;230:634–649.  
 [2] Munoz V, Thompson PA, Hofrichter J, and Eaton WA. Folding dynamics and mechanism of beta-hairpin formation. *Nature* 1997;390:196–199.

[3] Duan Y, and Kollman PA. Pathways to a protein folding intermediate observed in a 1-microsecond simulation in aqueous solution. *Science* 1998;282:740–744.  
 [4] Munoz V, Henry ER, Hofrichter J, and Eaton WA. A statistical mechanical model for beta-hairpin kinetics. *Proc Natl Acad Sci USA* 1998;95:5872–5879.  
 [5] Kolinski A, Ilkowski B, and Skolnick J. Dynamics and



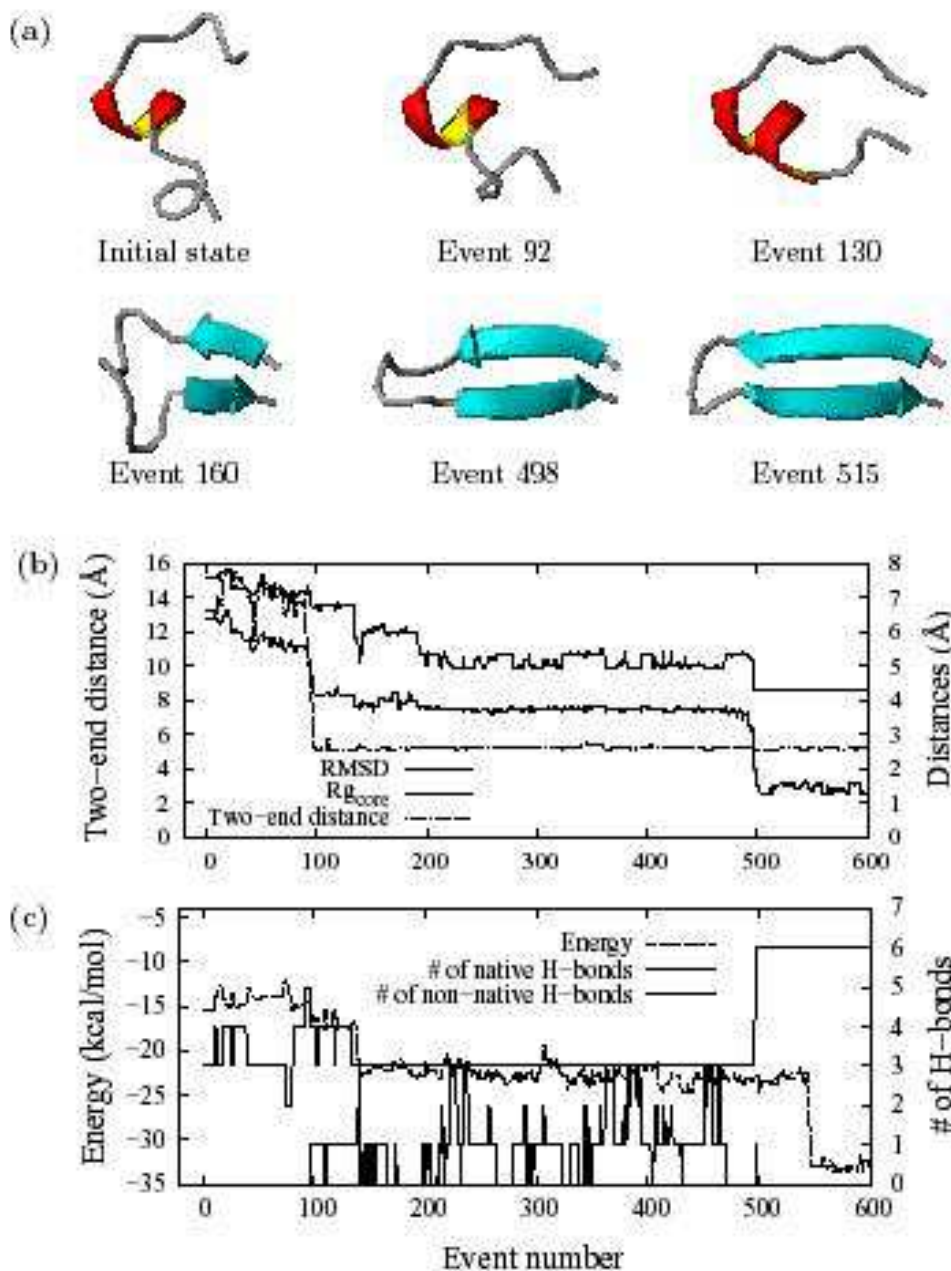


FIG. 10: A detailed analysis of a trajectory resulting in the fully  $\beta$ -hairpin at 300 K, starting from a semi-helical structure. In this initial state, the 14 pairs of  $(\phi, \psi)$  values, excluding residues Gly41 and Glu56, are  $(-63^\circ, 121^\circ)$ ,  $(-63^\circ, -27^\circ)$ ,  $(-65^\circ, 98^\circ)$ ,  $(-71^\circ, -10^\circ)$ ,  $(-48^\circ, 145^\circ)$ ,  $(-51^\circ, -61^\circ)$ ,  $(-56^\circ, -48^\circ)$ ,  $(-51^\circ, -55^\circ)$ ,  $(-61^\circ, -51^\circ)$ ,  $(-61^\circ, 94^\circ)$ ,  $(-63^\circ, -48^\circ)$ ,  $(-54^\circ, -43^\circ)$ ,  $(-59^\circ, -58^\circ)$ ,  $(-74^\circ, 80^\circ)$ .  $(\phi, \psi)$  values near  $(-60^\circ, -45^\circ)$  are typical for  $\alpha$ -helices. (a) Six snapshots. (b)  $C_\alpha$ -rmsd from 2GB1 structure of the hairpin, radius of gyration of the hydrophobic core  $Rg_{core}$ , and the two-end distance as a function of accepted event number. (c) Total energy, number of all the native and non-native H-bonds in each sampled conformation as a function of accepted event number.

thermodynamics of beta-hairpin assembly: insights from various simulation techniques. *Biophys J* 1999;77:2942–2952.

[6] Klimov DK, and Thirumalai D. Mechanisms and kinetics of  $\beta$ -hairpin formation. *Proc Natl Acad Sci USA* 2000;97:2544–2549.

[7] Tsai J, and Levitt M. Evidence of turn and salt bridge contributions to  $\beta$ -hairpin stability: MD simulations of

C-terminal fragment from the B1 domain of protein G. *Biophys Chem* 2002;101-102:187–201.

[8] Zagrobcic B, Sorin EJ, and Pande V.  $\beta$ -hairpin folding simulations in atomistic detail using an implicit solvent model. *J Mol Biol* 2001;313:151–169.

[9] Zhou R, Berne BJ, and Germain R. The free energy landscape for  $\beta$  hairpin folding in explicit water. *Proc Natl Acad Sci USA* 2001;98:14931–14936.

- [10] Zhou Y, and Linhananta A. Role of hydrophilic and hydrophobic contacts in folding of the second  $\beta$ -hairpin fragment of protein G: molecular dynamics simulation studies of an all-atom model. *Proteins* 2002;47:154–162.
- [11] Pande VS, and Rokhsar DS. Molecular dynamics simulations of unfolding and refolding of a beta-hairpin fragment of protein G. *Proc Natl Acad Sci USA* 1999;96:9062–9067.
- [12] Lee J, and Shin S. Understanding  $\beta$ -hairpin formation by molecular dynamics simulations of unfolding. *Biophys J* 2001;81:2507–2516.
- [13] Dinner AR, Lazaridis T, and Karplus M. Understanding  $\beta$ -hairpin formation. *Proc Natl Acad Sci USA* 1999;96:9068–9073.
- [14] García AE, and Sanbonmatsu KY. Exploring the energy landscape of a  $\beta$ -hairpin in explicit solvent. *Proteins* 2001;42:345–354.
- [15] Ma B, and Nussinov R. Molecular dynamics simulations of a beta-hairpin fragment of protein G: balance between side-chain and backbone forces. *J Mol Biol* 2000;296:1091–1104.
- [16] Irbäck A, Samuelsson B, Sjunnesson F, and Wallin S. Thermodynamics of  $\alpha$ - and  $\beta$ -structure formation in proteins. *Biophys J* 2003;85:1466–1473.
- [17] Fersht AR. On the simulation of protein folding by short time scale molecular dynamics and distributed computing. *Proc Natl Acad Sci USA* 2002;99:14122–14125.
- [18] Barkema GT, and Mousseau N. Event-based relaxation of continuous disordered systems. *Phys Rev Lett* 1996;77:4358–4361.
- [19] Barkema GT, and Mousseau N. Identification of relaxation and diffusion mechanisms in amorphous silicon. *Phys Rev Lett* 1998;81:1865–1868.
- [20] Forcellino F, and Derreumaux P. Computer simulations aimed at structure prediction of supersecondary motifs in proteins. *Proteins* 2001;45:159–166.
- [21] Wei G, Mousseau N, and Derreumaux P. Exploring the energy landscape of proteins: A characterization of the activation-relaxation technique. *J Chem Phys* 2002;117:11379–11387.
- [22] Bonvin AM, and van Gunsteren WF.  $\beta$ -hairpin stability and folding: molecular dynamics studies of the first  $\beta$ -hairpin of tendamistat. *J Mol Biol* 2000;296:255–268.
- [23] Wang H, Varady J, Ng L, and Sung S. Molecular dynamics simulations of  $\beta$ -hairpin folding. *Proteins* 1999;37:325–333.
- [24] Wei G, Derreumaux P, and Mousseau N. Sampling the complex energy landscape of a simple  $\beta$ -hairpin. *J Chem Phys* 2003;119:6403–6406.
- [25] Malek R, and Mousseau N. Dynamics of Lennard-Jones clusters: A characterization of the activation-relaxation technique. *Phys Rev E* 2000;62:7723–7728.
- [26] Mousseau N, Derreumaux P, Barkema GT, and Malek R. (2001). Sampling activated mechanisms in proteins with the activation-relaxation technique. *J Mol Graph Model* 2001;19:78–86.
- [27] Lanczós C. *Applied Analysis*. Dover, New York; 1988.
- [28] Munro LJ, and Wales DJ. Defect migration in crystalline silicon. *Phys Rev B* 1999;59:3969–3980.
- [29] Derreumaux P. From polypeptide sequences to structures using Monte Carlo simulations and an optimized potential. *J Chem Phys* 1999;11:2301–2310.
- [30] Derreumaux P. Generating ensemble averages for small proteins from extended conformations by monte carlo simulations. *Phys Rev Lett* 2000;85:206–209.
- [31] Gronenborn AM, and et al. A novel, highly stable fold of the immunoglobulin in binding domain of streptococcal protein-G. *Science* 1991;253:657–661.
- [32] Kabsch W, and Sander C. Dictionary of protein secondary structure: pattern recognition of H-bond and geometrical features. *Biopolymers* 1983;22:2577–2637.
- [33] Koradi R, Billeter M, and Wuthrich K. Molmol: A program for display and analysis of macromolecular structures. *J Mol Graphics* 1996;14:51–55.
- [34] Kamiya N, Higo J, and Nakamura H. Conformational transition states of  $\beta$ -hairpin peptide between the ordered and disordered conformations in explicit water. *Protein Sci* 2002;11:2297–2307.
- [35] Ma B, and Nussinov R. Energy landscape and dynamics of the  $\beta$ -hairpin G peptide and its isomers: Topology and sequences. *Protein Sci* 2003;12: 1882–1893.
- [36] Daura X, van Gunsteren WF, and Mark AE. Folding-unfolding thermodynamics of a heptapeptide from equilibrium simulations. *Proteins* 1999;34:269–280.
- [37] Derreumaux P, and Schlick T. The loop opening/closing motion of the enzyme triosephosphate isomerase. *Biophys J* 1998;74:72–81.
- [38] Searle MS, Williams DH, and Packman LC. A short linear peptide derived from the N-terminal sequence of ubiquitin folds into a water-stable non-native beta-hairpin. *Nat Struct Biol* 1995;2:999–1006.
- [39] Ramirez-Alvarado M, Kortemme T, Blanco FJ, and Serrano L. (1999). beta-hairpin and beta-sheet formation in designed linear peptides. *Bioorganic Medicinal Chemistry* 7, 93–103.
- [40] Humphrey D, Duggan C, Saha D, Smith D, and Käs J. Active fluidization of polymer networks through molecular motors. *Nature* 2002;416:413–416.